ENHANCED DIELECTRIC AND PHOTOCATALYTIC BEHAVIOUR OF Dy-Co CO-DOPED MULTIFERROIC BiFeO₃ NANOPARTICLES

A. SHABBIR[a], Z. A. GILANI[b], A. NAWAZ[c], M. F. WARSI[a*], M. A. KHAN[c], S. NAZIR[a], M. F. A. ABOUD[*d,e]

[a]*Department of Chemistry, Baghdad-ul-Jadeed Campus, The Islamia University of Bahawalpur, Bahawalpur-63100, Pakistan*
[b]*Department of Physics, Balochistan University of Management Sciences and Information Technology, Quettea-87300, Pakistan*
[c]*Department of Physics, Baghdad-ul-Jadeed Campus, The Islamia University of Bahawalpur, Bahawalpur-63100, Pakistan*
[d]*Sustainable Energy Technologies (SET) center, College of Engineering, King Saud University, PO-BOX 800, Riyadh 11421, Kingdom of Saudi Arabia*
[e]*Mining, Metallurgical and Petroleum Engineering Department, Faculty of Engineering, Al-Azhar University, Nasr City, Cairo 11371, Egypt*

Dysprosium and cobalt co-doped bismuth ferrites (BiFeO₃) were successfully synthesized by co-precipitation method. $Bi_{1-x}Dy_xCo_yFe_{1-y}O_3$ (where x= 0.00, 0.01, 0.02, 0.03, 0.04, 0.05 and y= 0.00, 0.10, 0.20, 0.30, 0.40, 0.50) nanoparticles were characterized by Thermogravimetric analysis (TGA), Scanning electron microscopy (SEM), X-ray diffraction analysis (XRD) and Fourier transform infrared spectroscopy (FTIR). Average particles size estimated by SEM was < 100 nm. XRD estimated the crystallite size in the range of 29-56 nm and confirmed the rhombohedral phase of $Bi_{1-x}Dy_xCo_yFe_{1-y}O_3$ nanoparticles unit cells. Application studies were done through dielectric parameters and photocatalysis experiments. Least dielectric constant observed was 12.673 for $Bi_{0.97}Dy_{0.03}Co_{0.3}Fe_{0.7}O_3$ and maximum of 27.64 for $Bi_1Dy_0Co_0Fe_1O_3$. Methylene blue was taken as representative organic dye for its photocatalytic degradation by $Bi_{1-x}Dy_xCo_yFe_{1-y}O_3$ nanoparticles under visible light. Dye was completely degraded under half an hour. Synthesized nanoparticles are magnetically separable therefore can easily be reclaimed for further usage as photocatalyst.

1. Introduction

The crystal structure and physical properties of BiFeO₃ based perovskitearemultiferroic materials have turned into the subject of serious examination amid late years, attributable to the considerable innovative capability of the materials for microelectronics and spintronic. The prevalence of bismuth ferrite, in which the stereo chemical movement of Bi lone electron pair offers ascend to ferroelectric polarization while the partially filled 3d orbitals of Fe^{3+} particles cause G-type antiferromagnetic order, is justified by its incredibly high transition temperatures. Due to multiferroic, photocatalytic and magnetic properties of BiFeO₃, it is valuable for applications in thin-film capacitor, nonvolatile memory, and nonlinear optics and photo electrochemical cells [1]. Researchers have used many strategies to obtain pure phase BiFeO₃ nanoparticles for their advanced technological applications. Mukherjee and co-workers fabricated bismuth ferrite nanoparticles doped by Yttrium by using latest Pechini technique and found it useful in photo catalytic decomposition of organic contamination [2]. Liu *et al.*utilized combination of electro-spinning and hydrothermal techniques with addition of glucose to prepare BiFeO₃ @ carbon core nano-fibers (BFO@CNFs) and observed that these particles can be reused.

These particles exhibited good photocatalytic activity [3]. Bernardo *et.al* synthesized multiferroic $BiFeO_3$ and observed three different phases during synthesis i.e. sillenite, mullite and an intermediate phase(perovskite type phase which result in the formation of $BiFeO_3$) [4].Apostolova*et al.*used Heisenberg and Ising model to study the effect of ion doping on the multi ferroicnano-particles and it was suggested that variation in defects increased the magnetization (M) and polarization (P) of $BiFeO_3$[5]. Wet chemical route was also adopted by many scientists to study the multiferroic properties along with doping effects and applications of $BiFeO_3$ nanoparticles [6-18]. Soltani*et al.*utilized the photocatalytic property of bismuth ferrite nanoparticles. Photo-catalyst with high purity was prepared by via ultra-sound under normal conditions and found maximum degradation efficiency in basic medium (pH=11)[19]. Abazariand co-workersprepared lanthanum ferrite nanoparticles at room temperature in CTAB emulsionnanoreactors.LaFeO$_3$ NPs with narrow band gap of 2.43eVwere used to degrade organic dye moleculesunder visible light and found to degrade more efficiently than commercial P-25 Titania powder [20].Liu *et al*synthesized multiferroic BiFeO3-(Na0.5 Bi0.5) TiO3 (BFO-NBT) nanopowder by sol-gel method and RhB was degraded under visible light. Researchers claim BFO-NBT a novel semiconductor visible light photo catalyst with narrow band gap, along with its wide range of applications for magneto electric devices[21].

Here in this manuscript, we report the synthesis of $Bi_{1-x}Dy_xCo_yFe_{1-y}O_3$ nanoparticles via facile wet chemical route, their structural elucidation and potential applications as high frequency devices fabrication and visible light driven photocatalyst materials.

2. Experimental

2.1. Synthesis of $Bi_{1-x}Dy_xCo_yFe_{1-y}O_3$ nanoparticles

$Bi_{1-x}Dy_xCo_yFe_{1-y}O_3$ nanoparticles were synthesized by chemical co-precipitation method [8, 16]. Solutions of following metal salts (used as received without any further purification) with desired molarities were prepared in deionized water and mixed in calculated ratios to form various compositions of $Bi_{1-x}Dy_xCo_yFe_{1-y}O_3$ where, x= 0.00, 0.01, 0.02, 0.03, 0.04, 0.05 and y= 0.00, 0.10, 0.20, 0.30, 0.40, 0.50: $Bi(NO_3).5H_2O$ (BDH, 98 %), $Fe(NO_3)_3.9H_2O$ (EMSURE, 99.0 %), $Dy(NO_3)_3$ (ALDRICH, 99.9 %), $(CH_3COO)_2Co.4H_2O$ (BDH, 99.9 %). Stirring was done at 50-60 °C to ensure homogenized mixing followed by maintaining the basic pH with freshly prepared ammonia solution. Precipitates of metal oxides were formed after 5-6 hrs continuous stirring, which were then dried, crushed and sintered in furnace at 950 °C for about 8 hrs.

2.2. Instrumentation

TGA was recorded through thermal analyzer (SDT Q600 V8.2 Build 100). Annealing of the samples was carried in controlled muffle Furnace Vulcan A-550.SEM analysis was carried out by using Jeol JSM-6490A Electron Microscope. XRD analysis was done by Philips X' Pert PRO 3040/60 diffractometer. FTIR spectra were recorded by SHMADZU IR spectrometer. The dielectric measurements were performed on Wayne Ker WK6500B precision equipment in the range of 1MHz to 3 GHz at 300 K. All UV-Visible measurements were carried at Cary 60, Dual Beam spectrophotometer in the range of 400-800 nm, using deionized water as reference.

3. Results and discussion

3.1 Thermogravimetric Analysis (TGA)

Total weight loss during analysis between the temperature range of 25-1000^{0}C was ~22% occurred through different phases. Firstly 14% of weight loss was observed from 70-110^{0}C which was due to loss of water contents subsequently the decomposition of nitrates caused 19% of weight loss until 330^{0}C. In next phase, ~20% weight loss was observed at around 800-820^{0}C which was due to the formation of oxides (Bi_2O_3,Fe_2O_3) from hydroxides of metals i.e. $Bi(OH)_3$ and $Fe(OH)_3$. Lastly at 950^{0}C the required perovskite phase was formed followed by no further weight loss upon heating [22]. The main purpose of TGA is to check the annealing temperature that was found to be

950^0C for BiFeO$_3$. Annealing temperature is defined as the temperature after which there is no chemical change in material occurs.
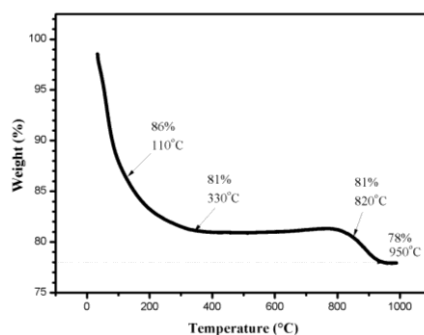
Fig. 1: TGA graph of "Bi$_1$Dy$_0$Co$_0$Fe$_1$O$_3$"nanoparticles.

3.2 Fourier-transform Infra-red Spectroscopy (FTIR)

FTIR spectroscopic analysis of prepared nanoparticles was performed within frequency range of 4000-400 cm^{-1} at room temperature, and recorded as frequency cm^{-1} (along x-axis) against percentage transmittance (along y-axis). The characteristic vibrational frequencies of metal oxygen bond in the range of ~400-600 cm^{-1} confirmed the formation of bismuth ferrite nanoparticles [23]. Fe-O stretching vibrations in FeO$_6$ octahedral unit occur at frequency ~550 cm^{-1} and that of Bi-O stretching vibrations at ~530 cm^{-1} which appear as a single broad band in FTIR spectrum of prepared BiFeO$_3$. Fe-O and Bi-O bending vibrations occur at ~440 cm^{-1} and ~450 of cm^{-1} respectively [17], and there appeared a broad band in spectrum (Figure 4.10) at frequency range of 420-450 cm^{-1} which is attributed for the bending vibrations of both Fe-O and Bi-O present in FeO$_6$ and BiO$_6$ octahedral structural unit respectively. Absorption band present at 574 cm^{-1} was may be due to out of phase vibrations of oxygen atoms in rhombohedral BFO. A very broad band at frequency 3000-3600 cm^{-1} corresponds to O-H stretching vibrations due to water molecules present. Absorption band at 1525 cm^{-1} is assigned to bending vibrations of H$_2$O [24].
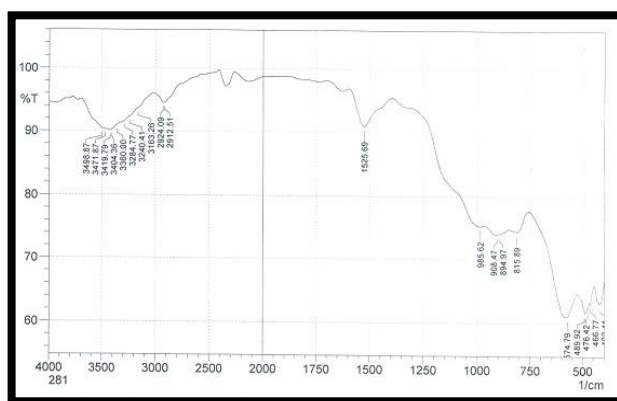
Fig. 2: FTIR spectrum of annealed BiFeO$_3$ nanoparticles without any substituent.

3.3 X-ray Diffraction Analysis (XRD)

XRD gives detailed information about the structure of unit cell and even chemical composition hence it was used to confirm the crystallographic structure. XRD patterns were matched with ICSD No.01-086-1518 [25]. Presence of sharp peaks confirmed the formation ofBi$_{1-x}$Dy$_x$Co$_y$Fe$_{1-y}$O$_3$ distorted rhombohedral structure. XRD pattern of BiFeO$_3$ also shows the formation of impure phases along with pure single phase crystalline nanoparticles. Peaks marked

with (*) shows the formation of mullite $Bi_2Fe_4O_9$ and sillenite $Bi_{25}FeO_{39}$ phase along with pure $BiFeO_3$ [4]. It is evident from Figure that the formation of impure phases with $2\Theta= 27^0$ and 28^0 prominently decreased as the amount of dopants i.e. Dy and Co increases. The sillenite and mullite phases again got high values in $Bi_{0.96}Dy_{0.04}Co_{0.4}Fe_{0.6}O_3$ and $Bi_{0.95}Dy_{0.05}Co_{0.5}Fe_{0.5}O_3$ where the dopants concentration was increased up to 5% and 50% for Dy and Co respectively. Therefore it is observed that doping of Dy(x) and Co(y) in $BiFeO_3$ nanoparticles with concentration up to x=0.03 and y=0.30 holds good for the formation of single phase bismuth ferrite nanoparticles. Moreover, crystallite size of nanoparticles was calculated by using Sherrer's formula which was found to be ~29-52 nm. As Dy was substituted at Bi site and Co at Fe site, the ionic radii of dopants may affect the crystallite size and other lattice parameters. There is a little difference in ionic radii of Dy^{+3} (0.0912nm) and Bi^{+3} (0.1030 nm); Co^{+3} (0.0610 nm) and Fe^{+3} (0.0645 nm) causing not any structural change.

Various physical parameters like lattice constants a, b, c and cell volume, were also calculated using cell software. Values of Lattice parameters a, b, c and cell volume confirmed that the prepared nanoparticles have distorted rhombohedral crystal structure with space group R3c (card no: 01-086-1518).
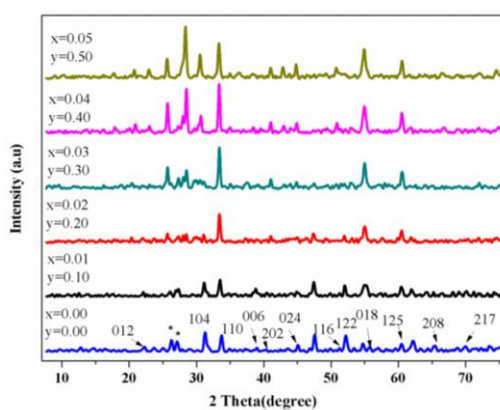
Fig. 3: XRD patterns of "$Bi_{1-x}Dy_xCo_yFe_{1-y}O_3$" nanoparticles

3.4 Scanning Electron Microscopic (SEM) Analysis

Scanning electron microscopic images of the Bi1-xDyxCoyFe1-yO3 nanoparticles were recorded on Jeol JSM-6490A Electron Microscope. The main purpose of the SEM analysis of was to probe the surface morphology of the nanomaterials. The grain size of the nanomaterials was also estimated from the SEM analysis.Typical SEM image of the $Bi_{1-x}Dy_xCo_yFe_{1-y}O_3$ nanoparticles is shown in Fig.4. The image shows that the grains are not properly spherical. Further the grains are also aggregated. The careful analysis of the SEM image estimated the average grain size < 100 nm.
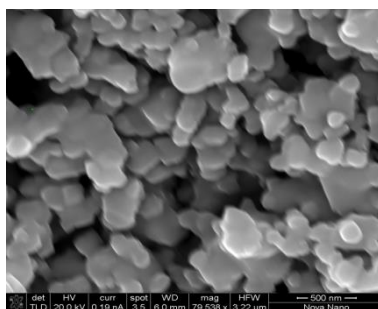
Fig. 4: SEM micrograph of $Bi_{0.97}Dy_{0.03}Co_{0.3}Fe_{0.7}O_3$ nanoparticles.

3.5 Dielectric measurements

Dielectric constant for each composition of prepared $Bi_{1-x}Dy_xCo_yFe_{1-y}O_3$ nanoparticles was measured as a function of frequency. It is evident that increase in AC current frequency lowers the value of dielectric constant. At lower frequency, the dielectric constant has highest value due to interfacial polarization and these polarizations respond very slowly to applied field that is why it has no effect at higher frequencies [26]. At higher frequency there are some resonance peaks, attributed to the resonance between electrical hopping ($Fe^{2+} \rightarrow Fe^{3+}$) and applied field resulting in an increase in dielectric constant value [27]. A decrease in dielectric constant value was observed as concentration of substituent metals was increased. It can be concluded that doping improves the dielectric nature of material by reducing the current leakage through oxygen vacancies and thus stabilizing the structure. At higher frequency, particles at grain boundaries resist the electronic flow (resistivity increases) and hence decreases the dielectric constant.
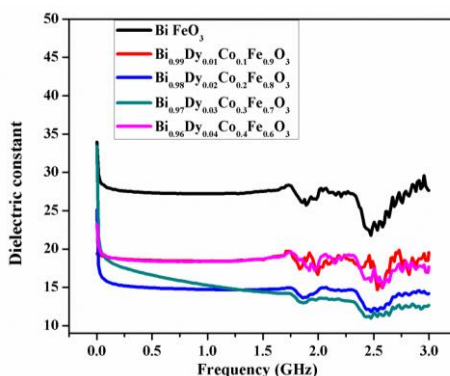
Fig. 5: Dielectric constant measurement of prepared $Bi_{1-x}Dy_xCo_yFe_{1-y}O_3$
nanoparticles as a function of frequency.

3.6 Photocatalysis of methylene blue dye by $Bi_{1-x}Dy_xCo_yFe_{1-y}O_3$ nanoparticles

Methylene blue is an organic dye that was selected as a reference organic contaminant. Most of the industry effluents contain untreated organic dyes which are carcinogenic in nature [28]. Methylene blue is also used in industries for dyeing purpose and it is highly water soluble. Among number of dyes methylene blue was elected due to its numerous beneficial features. Such as it was highly soluble in water, easily available, not much expensive therefore affordable to use, detection of result become easy due to its clearly detectable coloring capacity and it absorbs light in visible region.

Methylene blue has maximum absorption at 665 nm which is its absorption maxima [29] with a shoulder absorption peak at 615nm. The 1ppm solution of methylene blue (non-degraded) showed maximum absorption of A=1.13.

One of the compositions of our synthesized $Bi_{1-x}Dy_xCo_yFe_{1-y}O_3$ nanoparticles was selected to examine photodegradation process of dye. Among all the compositions, $Bi_{0.97}Dy_{0.03}Co_{0.3}Fe_{0.7}O_3$ nanoparticles was selected on the basis of magnetic property tested by using magnetic bar through conventional method. Photocatalytic degradation process was performed by using $Bi_{0.97}Dy_{0.03}Co_{0.3}Fe_{0.7}O_3$ nanoparticles as photocatayst to degrade methylene blue under visible light. For comparative purpose, UV-Visible spectrum of methylene blue after every 3 minutes of photocatalytic treatment was recorded to show systematic degradation of dye.The absorption maxima of methylene blue got decreased its value after every interval and reached the lowest value under 24 minutes, by the use of $Bi_{1-x}Dy_xCo_yFe_{1-y}O_3$ nanoparticlesas photocatalystunder visible light.
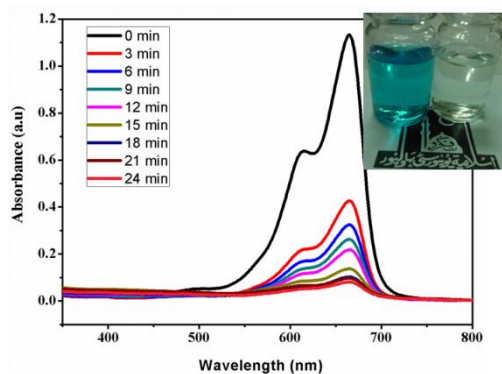
Fig. 6: UV-Vis absorption spectra of methylene blue solution catalyzed
by $Bi_{1-x}Dy_xCo_yFe_{1-y}O_3$ nanoparticles (0-24min)

Degradation rate was also calculated by using exact values of both absorption peaks (665 and 615nm) for methylene blue under visible light. Degradation i.e. A/A0 as a function of time showed the clear decrease in absorption with the passage of time (Figure 7). It was seen that after first time interval, degradation rate was high which get lowers by time. That may be attributed to the efficiency of photocatalyst which was maximum at the start of experiment and decreases its efficiency with time due to lots of reasons may be. Same pattern was observed as degradation rate was calculated for absorption at 615nm.
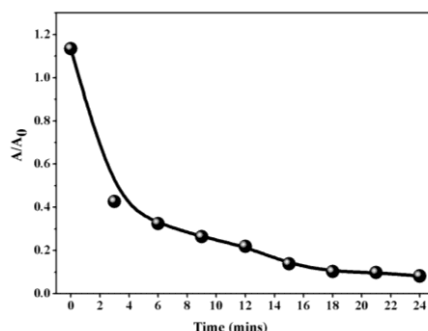
Fig 7: Degradation rate of methylene blue vs time (at ʎ 665 nm).

4. Conclusions

$Bi_{1-x}Dy_xCo_yFe_{1-y}O_3$ nanoparticles were prepared by wet chemical route i.e. co-precipitation and characterized by TGA, SEM, FTIR, and XRD. The XRD data also revealed the formation of second phase. Crystallite size estimated by XRD and grain size estimated by SEM was found < 100 nm. Application studies of these particles were done by dielectric and photocatalytic studies. Dielectric parameters were decreased by substitution of dysprosium and cobalt. The particles showed excellent photocatalytic activity.

References

[1] V.A. Khomchenko, V.V. Shvartsman, P. Borisov, W. Kleemann, D.A. Kiselev, I.K. Bdikin, J.M. Vieira, A.L. Kholkin, Acta Materialia **57**, 5137 (2009).

[2] A. Mukherjee, S.M. Hossain, M. Pal, S. Basu, Appl Nanosci **2**, 305 (2012).

[3] Y. Liu, R. Zuo, S. Qi, Journal of Molecular Catalysis A: Chemical **376**,1 (2013).

[4] M. Bernardo, T. Jardiel, M. Peiteado, A. Caballero, M. Villegas, Journal of the European Ceramic Society **31**, 3047 (2011).

[5] I. Apostolova, J.M. Wesselinowa, Journal of Magnetism and Magnetic Materials **321,** 2477 (2009).

[6] R. Safi, H. Shokrollahi, Physics, Progress in Solid State Chemistry **40**, 6 (2012).

[7] S.M. Selbach, T. Tybell, M.-A. Einarsrud, T. Grande, Chemistry of Materials **21**, 5176 (2009).

[8] H. Ke, W. Wang, Y. Wang, J. Xu, D. Jia, Z. Lu, Y. Zhou, Journal of Alloys and Compounds **509**,2192 (2011).

[9] P. Lin, S. Cui, X. Zeng, H. Huang, S. Ke, Journal of Alloys and Compounds **600**, 118 (2014).

[10] W. Mao, X. Wang, Y. Han, X.a. Li, Y. Li, Y. Wang, Y. Ma, X. Feng, T. Yang, J. Yang, W. Huang, Journal of Alloys and Compounds **584**,520 (2014).

[11] P. Priyadharsini, A. Pradeep, B. Sathyamoorthy, G. Chandrasekaran, Journal of Physics and Chemistry of Solids **75**,797 (2014).

[12] T.D. Rao, T. Karthik, S. Asthana, Journal of Rare Earths **31**, 370 (2013).

[13] M. Sakar, S. Balakumar, P. Saravanan, S.N. Jaisankar, Materials Research Bulletin **48,** 2878(2013).

[14] S.M. Selbach, M.A. Einarsrud, T. Tybell, T. Grande, Journal of the American Ceramic Society **90**, 3430 (2007).

[15] S.M. Selbach, M.-A. Einarsrud, T. Grande, Chemistry of Materials **21**, 169 (2008).

[16] M.Y. Shami, M.S. Awan, M. Anis-ur-Rehman, Journal of Alloys and Compounds **509**, 10139(2011).

[17] M. Arora, S. Chauhan, P.C. Sati, M. Kumar, S. Chhoker, Ceramics International **40,** 13347 (2014).

[18] S. Chauhan, M. Arora, P.C. Sati, S. Chhoker, S.C. Katyal, M. Kumar, Ceramics International **39,** 6399(2013).

[19] T. Soltani, M.H. Entezari, Journal of Molecular Catalysis A: Chemical **377**,197 (2013).

[20] R. Abazari, S. Sanati, L.A. Saghatforoush, Materials Science in Semiconductor Processing **25**, 301(2014).

[21] H. Liu, Y. Guo, B. Guo, D. Zhang, Solid State Sciences **19**, 69(2013).

[22] Z. Anwar, M. Azhar Khan, A. Mahmood, M. Asghar, I. Shakir, M. Shahid, I. Bibi, M. Farooq Warsi, Journal of Magnetism and Magnetic Materials **355**,169 (2014).

[23] A. Z. Simões, G. Biasotto, C. R. Foschini, S. G. Antônio, M. A. Zaghete, J. A. Varela, Processing and Application of Ceramics **5**, 171 (2011).

[24] P.H. Suresha, Ramani, M.C. Radhakrishna, B. Angadi, J.T. Devaraj, Indian journal of Engeneering and Material sciences **19,** 196 (2012).

[25] I. Sosnowska, R. Przeniosło, P. Fischer, V.A. Murashov, Journal of Magnetism and Magnetic Materials **160**,384 (1996).

[26] A. Gupta, R. Chatterjee, Journal of Magnetism and Magnetic Materials 322,1020 (2010).

[27] Z. Anwar, M. A. Khan, I. Ali, M. Asghar, M. Sher, I. Shakir, M. Sarfraz, M. F. Warsi, Journal of Ovonic Research **10,** 265 (2014).

[28] U.I. Gaya, A.H. Abdullah, Journal of Photochemistry and Photobiology C: Photochemistry Reviews **9**, 1 (2008).

[29] J. Yao, C. Wang, International Journal of Photoenergy **2010**, 643182 (2010).